Research Article | Vol. 10, No. 4 | 1 Apr 2019 | BIOMEDICAL OPTICS EXPRESS 1627
Biomedical Optics EXPRESS

Optical properties of adult *Drosophila* brains in one-, two-, and three-photon microscopy

KUO-JEN HSU,[1,2] YEN-YIN LIN,[2,7] ANN-SHYN CHIANG,[2,3,4,5,8] AND SHI-WEI CHU[1,6,9]

[1]*Department of Physics, National Taiwan University, Taipei 10617, Taiwan*
[2]*Brain Research Center, National Tsing Hua University, Hsinchu 30013, Taiwan*
[3]*Institute of Systems Neuroscience, National Tsing Hua University, Hsinchu 30013, Taiwan*
[4]*Department of Biomedical Science and Environmental Biology, Kaohsiung Medical University, Kaohsiung 80780, Taiwan*
[5]*Kavli Institute for Brain and Mind, University of California at San Diego, La Jolla, CA 92093-0526, USA*
[6]*Molecular Imaging Center, National Taiwan University, Taipei 10617, Taiwan*
[7]*yylin@life.nthu.edu.tw*
[8]*aschiang@life.nthu.edu.tw*
[9]*swchu@phys.ntu.edu.tw*

Abstract: *Drosophila* is widely used in connectome studies due to its small brain size, sophisticated genetic tools, and the most complete single-neuron-based anatomical brain map. Surprisingly, even the brain thickness is only 200-μm, common Ti:sapphire-based two-photon excitation cannot penetrate, possibly due to light aberration/scattering of trachea. Here we quantitatively characterized scattering and light distortion of trachea-filled tissues, and found that trachea-induced light distortion dominates at long wavelength by comparing one-photon (488-nm), two-photon (920-nm), and three-photon (1300-nm) excitations. Whole-*Drosophila*-brain imaging is achieved by reducing tracheal light aberration/scattering via brain-degassing or long-wavelength excitation at 1300-nm. Our work paves the way toward constructing whole-brain connectome in a living *Drosophila*.

1. Introduction

Drosophila is an important model animal to study connectomics since its brain is complex with 10^5 neurons but still small enough to be completely mapped by optical microscopy with single-cell resolution. Compared to other model animals, the genetic tool box is more complete with *Drosophila*, and a connectome map based on *in vitro* structural registration of more than 30,000 cells [1,2] and 3D reconstruction of serial EM sections [3] has been established, serving as an invaluable reference for connectomics study. To study the structural/functional connectome, two-photon fluorescence (2PF) microscopy is now the most popular tool because of its advantages on low photobleaching and phototoxicity, subcellular spatial resolution, and deep penetration depth [4]. When observing living mouse or zebrafish brain with 2PF microscopy, the penetration depth approaches 1 mm, which is typically limited to about five scattering lengths [4,5]. However, even using the same fluorophore and excitation wavelength, the reported imaging depths in a living *Drosophila* brain are much more limited. For example, when imaging GCaMP with excitation wavelength around 920-nm, activities from mushroom bodies (MB) had been recorded at only several tens of micrometers in depth [6,7]. Using the same combination of laser and probe, the neuronal activities from antennal lobes (AL) are obtained with imaging depth less than 100 μm [8–11]. Although the thickness of a *Drosophila* brain is only about 200 μm, which is much smaller than the typical imaging depth of 2PF microscopy in other model animals like mouse and zebrafish, to the best of our knowledge, no study has demonstrated *in vivo* whole-brain imaging in *Drosophila* with single-cell resolution, nor has characterized the image attenuation

#348348 https://doi.org/10.1364/BOE.10.001627
Journal © 2019 Received 25 Oct 2018; revised 23 Jan 2019; accepted 17 Feb 2019; published 5 Mar 2019

Biomedical Optics EXPRESS

of a living *Drosophila* brain. The whole-brain observation capability is a major milestone toward establishing complete connectome in this model animal.

The underlying difficulty of living *Drosophila* whole-brain imaging is that, different from mouse and zebrafish, where blood vessels are responsible for oxygen exchange, air vessels, i.e., tracheae, are in charge of oxygen exchange in *Drosophila* brains. The micro-tracheae in the brain are a few micrometers in diameter [12], comparable to near infrared wavelengths, and thus induce extraordinarily strong light aberration/scattering from the air/tissue interface since the refractive index (RI) difference between air and tissue is much larger than that between blood and tissue. This tracheae-induced light aberration/scattering impedes deep tissue observations inside a living *Drosophila* brain. However, the optical properties of trachea-filled tissues have not been well studied. Therefore, the aim of this work is to unravel the optical effect of tracheae, and to design a suitable method to increase imaging depth in trachea-filled tissues.

To increase imaging depth in living animals, there are several known approaches. For example, photo-activatable fluorophores (PAFs) have been used to suppress out-of-focus fluorescence [13], and high-energy lasers were used to enhance excitation efficiency at deep tissue [14]. However, long converting time is required for PAFs, which is unfavorable to observe fast neural activities such as calcium dynamics, and high-energy lasers are potentially harmful due to multiphoton ionization. Adaptive optics (AO) is able to correct tissue-induced light distortion, and has demonstrated significant image contrast and depth enhancement [15–18]. Nevertheless, the best depth achieved by AO in a living *Drosophila* brain to date is still less than 100 μm [18], since the distortion inside the insect's brain is much larger than that of vertebrate's brain (RI difference between air and tissue is at least ~1 order of magnitude larger than that between blood and tissue). In addition, typically AO does not compensate the scattering effect [16], which limits its impact in improving the imaging depth in *Drosophila*.

On the other hand, long excitation wavelength is well known to greatly improve penetration depth by substantially reducing scattering [5,19–21]. In addition, the phase error caused by aberration (i.e., wavefront distortion) is inversely proportional to the excitation wavelength. The long wavelength approach is expected to reduce the amount of light distortion caused by the RI difference, and thus enhancing imaging depth. Furthermore, high-order optical nonlinear excitations, such as three-photon absorption, are often combined with long wavelength, thus providing better excitation confinement, i.e. better optical sectioning capability, than 2PF, to improve image contrast in deep tissue. Combining these factors together, long wavelength excitation is promising for whole-brain imaging in *Drosophila*.

Here, two approaches are adopted to achieve whole-brain observation in a *Drosophila* brain. The first one is to pump out air inside the tracheae, i.e. degassing. Since the tracheae-induced light aberration/scattering is largely removed in the degassed brain, 2PF microscopy penetrates through the whole brain. However, the *Drosophila* is not alive after degassing. To achieve whole-brain observation with *in vivo* capability, the second approach is to use three-photon imaging based on excitation wavelength at 1300-nm in a GFP-labeled living *Drosophila* brain. The three-photon fluorescence (3PF) method provides exceptional excitation confinement and simultaneously reduced light aberration/scattering, thus allows high-contrast and high-resolution image throughout the whole brain. The accompanying third harmonic generation (THG) modality provides detailed map of the densely distributed tracheae in the brain, useful for structure-function studies.

Furthermore, the optical attenuations of the *Drosophila* brains at various wavelengths are characterized, via 1PF (488-nm), 2PF (920-nm) and 3PF (1300-nm) excitation modalities. For the first time, the attenuations contributed from tracheae are quantitatively determined. We show that at short wavelength, scattering is the dominating attenuation; while at long wavelength, the contribution of trachea-induced light distortion can exceed that of scattering, and become the main impeding factor of whole-brain observation in *Drosophila* brains.

Biomedical Optics EXPRESS

2. Methods

2.1 Microscope setups

For 1PF and 2PF imaging, the imaging was done on a commercial microscope LSM 780 (Zeiss, Germany). The built-in laser (488-nm) and photomultiplier tube was used to single-photon excitation and signal detection. A water immersion objective was used (Olympus, XLPlan N, 25 × NA 1.05) for its high transmission in both visible and IR wavelength ranges. A pinhole with ~60 μm diameter was used to achieve optical sectioning. The image formation was done by the controlling software Zen (Zeiss, Germany).

For 2PF and 3PF *in vivo* imaging, the setup was similar to that done by Ouzounov et al [22]. A home-built laser-scanning microscope that is compatible to long wavelength excitation is constructed. A Ti: sapphire laser at 920-nm with an 80 MHz repetition rate, and an optical parametric amplifier at 1300-nm with a 400 kHz repetition rate, were used as excitation sources of 2PF and 3PF respectively. The same water immersion objective as single-photon microscope was used. The power levels for both lasers after the objective were limited to less than 20 mW for all imaging depths. The fluorescence and THG signals were epi-collected with a dichroic beamsplitter (Semrock, FF705-Di01-25 × 36), and then detected by a GaAsP photomultiplier tube (Hamamatsu, H7422-40) and a bialkali photomultiplier tube (Hamamatsu, R7600-200) in non-descanned configurations to maximize the collection efficiency. A 488-nm dichroic beamsplitter (Semrock, Di02-R488-25 × 36) was used to split the fluorescence and THG signals, which were further separated by a 520/60 band-pass filter (BPF, transmission at center 520-nm, FWHM 60 nm) for the fluorescence and a 420/40 BPF for the THG. A living *Drosophila* was fixed and placed onto a motorized stage (M-285, Sutter Instrument). A computer running the ScanImage 3.8 under Matlab (MathWorks) was used to synchronize the stage movement and image acquisition. The signal current from the detectors was converted to voltage, amplified and low-pass filtered by a transimpedance amplifier (Hamamatsu, C9999) and another 1.9 MHz low-pass filter (BLP-1.9 + , Minicircuits). Analog-to-digital conversion was performed by a data acquisition card (PCI-6115, National Instruments).

2.2 Sample preparations

All the sample preparation methods followed the protocol of previous publication on *in vivo Drosophila* brain imaging [23]. The samples were adult, female *Drosophila* between 5 and 10 days old. GFP was pan-neuronal expressed by genetic drivers (Gal4-elav.L/CyO × UAS-EGFP and Gal4-elav/UAS-mGFP). The living *Drosophila* was immobilized in a pipette tip with volume 100 μL after anesthetized by ice bathing. A window was cut into the head by using fine tweezers, after placing a drop of Ca^{2+}-free saline on the brain to prevent desiccation, and fat bodies above the brain were removed, under a stereomicroscope. The dissection saline was then replaced with a drop of Ca^{2+}-containing saline (108 mM NaCl, 5 mM KCl, 2 mM $CaCl_2$, 8.2 mM $MgCl_2$, 4 mM $NaHCO_3$, 1 mM NaH_2PO_4, 5 mM trehalose, 10 mM sucrose, and 5 mM HEPES [pH 7.5, 265 mOsm]). No cover glass was placed between the brain and the objective.

To check the optical effect caused by the tracheae structure, degassing the *Drosophila* brain was performed by pumping out the air inside tracheae. The degassing protocol followed the previous publication of *in situ Drosophila* brain imaging [24]. The degassing protocol started from immersing the *Drosophila* in 4% paraformaldehyde and 2% triton, expelling air in tracheae by using a vacuum chamber that was depressurized to – 72-mmHg for 2.5 minutes, wait for 1.5 minutes, and then releasing to normal pressure for 2 minutes. The degassing process was completed by repeating the above procedure 4 times. After degassing, the same microsurgery preparation was performed, and observed under the same microscope.

Biomedical Optics EXPRESS

2.3 Signal analyses

To quantify the optical properties of bio-tissues, this section explains how to derive the attenuation coefficients (μ_{att}), which is the inverse value of attenuation length (l_a), i.e., $\mu_{att} = l_a^{-1}$. The calculation of attenuation length inside a biological tissue has been detailed in an earlier work [5]. The well-known light attenuation equation is:

$$I(d) = I_0 e^{-d/l_a} = I_0 e^{-\mu_{att} \times d} \tag{1}$$

where $I(d)$ is the excitation intensity at imaging depth of d, and I_0 is the intensity at tissue surface. With fluorescence excitation processes, the n-th order fluorescence intensity, $F^{(n)}(d)$, is related to the excitation intensity as:

$$F^{(n)}(d) \propto (I(d))^n \tag{2}$$

For 1PF, 2PF and 3PF, n equals 1, 2 and 3, respectively. Combining Eqs. (1) and 2, $F^{(n)}(d)$ is obtain in Eq. (3),

$$F^{(n)}(d) = a \times e^{-n \times \mu_{att} \times d} \tag{3}$$

where a is a proportional constant. $F^{(n)}(d)$ and d are determined experimentally, and μ_{att} can be obtained from their dependencies. More explicitly, by taking the natural logarithmic value of both sides in Eq. (3), it becomes,

$$\ln(F^{(n)}(d)) = \ln(a) - n \times \mu_{att} \times d \tag{4}$$

By plotting the dependence of $\ln(F^{(n)}(d))$ on d (will be shown in Fig. 2), the decay slopes of the curves are $-n \times \mu_{att}$. Therefore, μ_{att} is determined by dividing the inverse value of the slopes over n. To obtain the decay slopes, it was done by linear regression fitting of the data points, and the fitting range were selected by the same criteria. They were all selected with the starting point of signal decay to the depth limit of the corresponding imaging modality. One additional note is since there are two imaging systems, 2PF *in vivo* experiments are performed in both systems to calibrate the attenuation value derived from different systems.

3. Results and discussions

Within a living brain, the 1PF images lose the image contrast at around 40 μm (Visualization 1), as no structures are visible in the brain center where the white arrow points in the 50-60 μm panel of Fig. 1(A). The arrowheads indicate structures that located at the edge of the brain. To verify the effect of trachea, a brain is degassed, i.e. air in tracheae is pumped out. Figure 1(B) shows that 1PF in the degassed brain provides much better contrast in the center of brain at the same depth, but cannot exceed 120-140 μm. The 1PF imaging depth of the degassed brain is comparable with that in mouse brains, which is mainly limited by scattering [4]. Comparing the results in Figs. 1(A) and 1(B), it is obvious that degassing removes the additional attenuation contributed by tracheae.

On the other hand, it is well known that using long excitation wavelengths with 2PF modality efficiently improves imaging depth, approaching 1 mm in mouse brains [4]. Using the same excitation wavelength (~920-nm) and fluorescent labeling (GFP families), Fig. 1(C) shows the 2PF imaging depth in a living *Drosophila* brain indeed increases compared to Fig. 1(A), but reaches less than 120-140 μm, which is not adequate to penetrate the whole brain, mainly due to the tracheae. By combining 2PF modality with a degassed brain, Fig. 1(D) presents the first whole-brain imaging in a *Drosophila*. Reasonable contrast and resolution (see inset in the bottom panel for resolving single neuron) are maintained throughout the nearly 200 μm depth, manifesting that the trachea-induced light aberration/scattering is the major restraint for deep-brain imaging in this model animal. However, please note that the

Biomedical Optics EXPRESS

animal is no longer alive after degassing. Moreover, the degassing process distorts the brain structures, making its association with the *Drosophila* structural connectome difficult.

In order to observe whole-brain of living *Drosophila*, 3PF at excitation wavelength ~1300-nm was adopted. Figure 1(E) shows that this imaging modality provides cellular resolution (inset in the bottom panel) throughout a living *Drosophila* brain. By associating with an existing *Drosophila* brain database (FlyCircuit, http://www.flycircuit.tw), several local processing units (LPUs) [1] at each depth ranges are identified in Figs. 1(A) - 1(E). Please note that although an elav promoter is used here, the genotype of Figs. 1(C) and 1(E) is slightly different from that of Figs. 1(A), 1(B) and 1(D), resulting in different visibility of neuropil structures. However, this should not affect the judgment of whole-brain penetrability.

During the three-photon excitation process, a complementary contrast, i.e. THG, is generated by the interfaces with RI differences, and thus is sensitive to the tissue/air boundaries in tracheae. Figure 1(F) shows that THG signals reveals the detailed distribution of tracheae, which are randomly distributed inside the brain and causing strong light aberration/scattering.

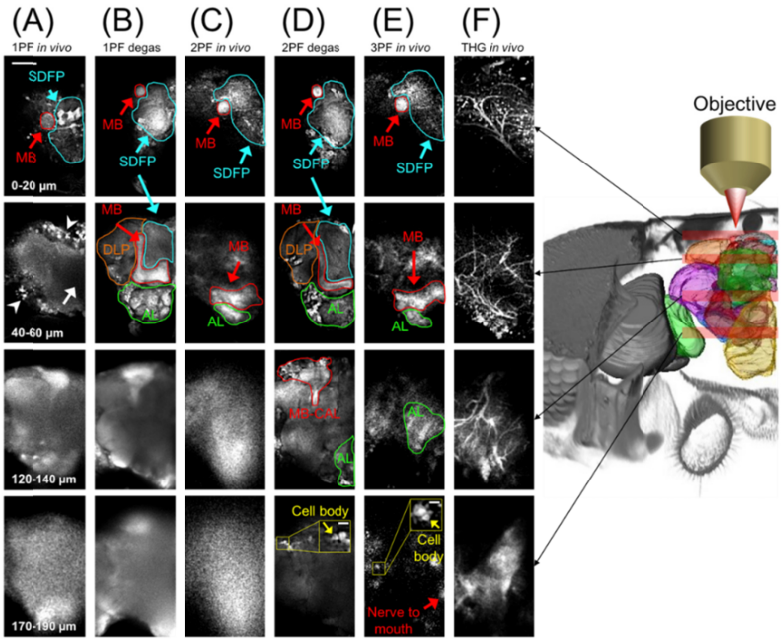

Fig. 1. Living and degassed *Drosophila* brain images under different imaging modalities. (A), (C) and (E) are 1PF, 2PF and 3PF images at 0-20, 40-60, 120-140 and 170-190 μm axial projected images of a living brain. (B) and (D) are 1PF and 2PF images of a degassed brain at the same depth ranges. Although brain-edge structures (arrowheads) are still visible at 40-60 μm depth in (A), the image loses contrast in brain center (white arrow). In the degassed brain, the penetration depth of 1PF is significantly improved in (B), but not approaching the bottom of brain. In (C), 2PF penetrates deeper than 1PF, but becomes blurry at depth beyond 100 μm. Whole-brain imaging is achieved in (D) by 2PF in a degassed brain. (E) shows only 3PF maintains contrast and reasonable resolution throughout the whole brain. The insets in the bottommost panels of (D) and (E) show clear cell bodies. (F) THG images, a complementary contrast with 3PF, show clear tracheae distribution. By comparing with structural connectome, several LPUs at corresponding depth ranges are annotated in (A) - (E), including MB: mushroom body, SDFP: superior dorsofrontal protocerebrum, AL: antennal lobe, DLP: dorsolateral protocerebrum, and CAL: calyx. All the images are intensity normalized with individually brightest 0.5% pixels. Scale bar: 50 μm for (A); 1 μm for insets of (D) and (E). Complete depth-images are given in Visualization 1, Visualization 2, and Visualization 3. Genotype: (A), (B) and (D) are Gal4-elav/UAS-mGFP, (C) and (E) are Gal4-elav.L/CyO × UAS-EGFP.

Biomedical Optics EXPRESS

To quantify signal attenuation coefficients (μ_{att}) of different imaging modalities, Figs. 2(A) - 2(C) show the decay of 1PF, 2PF, and 3PF signals, corresponding to Figs. 1(A) - 1(E) respectively, within living or degassed brains. To prevent inappropriate estimation of μ_{att}, the signal extraction should avoid bright structures as shown by the white box in the inset of Fig. 2(A). In addition, to evaluate the potential influences from chemical treatments (paraformaldehyde and triton), we have made a control experiment to compare the difference between live brain and those treated by paraformaldehyde and triton without the degassing step. From Fig. 2(A), the signal decay of the chemically treated brain (orange curve) overlaps with that of living brain (black curve), suggesting that paraformaldehyde and 2% triton treatment does not significantly affect optical properties of *Drosophila* brain.

By linear fitting of the individual signals as shown by red and pink lines for *in vivo* and degassed samples, their μ_{att} in Fig. 2 is derived respectively (see section 2.3 for methods). Apparently, both degassing and long wavelength excitation help to reduce μ_{att} significantly. The μ_{att} of 2PF and 3PF are around one-third and one-quarter of that of 1PF in living *Drosophila* brains, while the lowest μ_{att} is provided by 2PF plus degassing. Comparing to mouse brain whose μ_{att} of 2PF and 3PF are less than one-third and one-eighth of 1PF [5], the influence of longer excitation wavelength is much smaller in *Drosophila* brains. To better understand the results, the μ_{att} has to be decomposed, as we explain in the following.

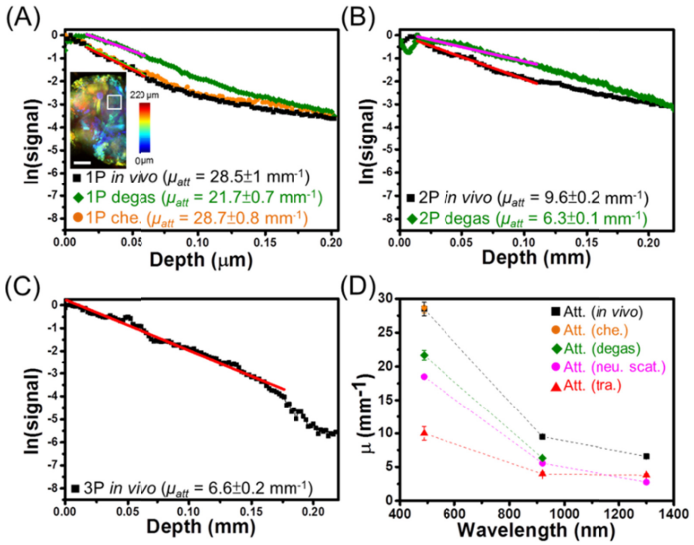

Fig. 2. 1PF, 2PF, and 3PF signal attenuations in living and degassed brains, and quantitative analysis on contributions from scattering and aberration. (A) and (B) show the semi-logarithmic plot of 1PF and 2PF signal attenuations with depth, inside a living (black) and degassed (green) brains, respectively corresponding to Figs. 1(A) - 1(D). The orange curve in (A) (1P che.) is a control experiment of chemically treated brain (paraformaldehyde and triton), but no degassing. (C) 3PF signal attenuation of a living brain in Fig. 1(E). The inset in (A) is a depth color-coded brain image that shows the area (white box) for signal extraction at different depths. The signals are obtained by averaging the brightest 1% pixels at different depths inside the white box. The red and pink lines in (A) - (C) are linear fits of the signals, and their corresponding attenuation coefficients (μ_{att}) are shown in the bottom. (D) Quantitative comparison of μ_{att} in living brains (black squares) and degassed brains (green diamonds) at each wavelength, and that from brain only treated by chemicals (orange circle), together with corresponding attenuations from mouse brains, i.e. neuron scattering (pink circles) and tracheae (red triangles). Scale bar in inset of (A): 50 μm. In the 1P and 2P degassed brain, 2 and 3 replicates are analyzed to confirm the attenuation coefficients. For the *in vivo* brain imaging of 2P and 3P, it is performed on the same *Drosophila*. Therefore, it should be beyond doubt that 3P penetrates deeper than 2P, without the need of more replicates.

Biomedical Optics EXPRESS

First of all, the absorption contribution should be negligible in our experiment. When the *Drosophila* brain is dissected out, the color is white, indicating that no strong absorption in the visible range. In addition, it is known that *Drosophila* trachea exhibits autofluorescence, but in our experiment when using 488-nm, no fluorescence from trachea is observed, again implying negligible absorption at this visible wavelength. Regarding to the infrared light region (920-nm and 1300-nm), the total attenuations are both much smaller than that of 488-nm, indicating that no strong absorption is presented at these wavelengths. Furthermore, for 920-nm excitation, the degassed attenuation agrees well with scattering model from mouse brain, further suggesting that absorption is not dominant.

In Fig. 2(D), the attenuation coefficients of *in vivo* and degassed brains are plotted in black and green, respectively. It is interesting to note that the attenuations of degassed brains are comparable to that of a mouse brain (pink circles), which is mostly contributed from scattering of neurons [5]. The slight difference may be due to the effect of residual wax in the tracheae. From the comparison of *in vivo Drosophila* brain (total attenuation, μ_{att}) and mouse brain (attenuation from neurons, μ_{neu}), the contribution of trachea $\mu_{tra} = \mu_{att} - \mu_{neu}$ is derived as red triangles in Fig. 2(D).

The results show that both μ_{neu} and μ_{tra} reduce with increasing wavelengths, with respectively λ^{-2} and $\lambda^{-0.9}$ dependencies as shown in Fig. 3. Since the attenuation of neuronal tissue μ_{neu} is dominated by scattering, which includes Rayleigh scattering (λ^{-4} dependence) and Mie scattering (λ^{-1} dependence), the λ^{-2} dependency should be a natural result of the mixture. On the other hand, the $\lambda^{-0.9}$ dependency suggests that μ_{tra} may not be governed by scattering, whose wavelength dependency should be between λ^{-4} and λ^{-1}, but by light distortion from air-tissue interfaces.

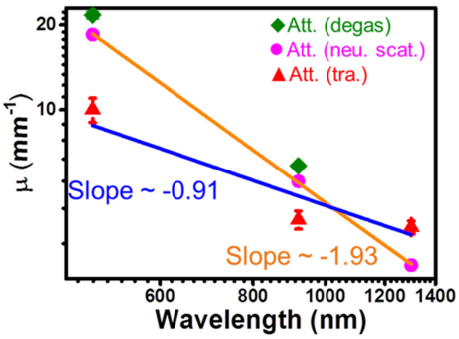

Fig. 3. Wavelength dependency of attenuations from neuronal scattering, trachea-induced light distortion and degassed *Drosophila* brain attenuations. By plotting in a log-log scale, the slope indicates the exponential power of neuronal scattering, which is about λ^{-2}. The result is reasonable since tissue scattering can be considered as a mixture of Mie scattering (λ^{-1} dependence) and Rayleigh scattering (λ^{-4} dependence). The slope of blue line points out that the power of trachea-contributed attenuation, which is around $\lambda^{-0.9}$.

To further confirm that scattering does not play the key role in the attenuation of the trachea-filled brain, we compare the 2PF μ_{att} of *Drosophila* and mouse in Fig. 2(D), the latter (~5.5 mm^{-1}) is around half of the former (~9.6 ± 0.2 mm^{-1}). Nevertheless, 2PF imaging in mouse brains typically reaches almost 1 mm, i.e. about five scattering lengths; while in living *Drosophila* brains, only about 100 μm, i.e. less than two attenuation lengths, is achieved. Similar situation occurs with the 3PF modality. The surprisingly limited penetration depth suggests that scattering does not dominate the attenuation, but the trachea-induced light distortion dictates, especially in multiphoton imaging cases. The trachea-induced light distortion have similar effect as blood vessels in mouse brain, which act like cylindrical lens that produce astigmatism and thus elongating the axial point-spread-function (PSF) [25]. It has been shown recently that wavefront distortion is the main factor to deform the PSF, not

Biomedical Optics EXPRESS

scattering [26,27]. Therefore, the limited depth is mainly due to that light distortion not only induce excitation intensity loss, but also strongly deteriorates the axial PSF as shown in Fig. 4. As a result, capability of 2PF optical sectioning quickly loses at relatively shallow region, leading to blurred images and considerably limited imaging depth, as manifested in Fig. 1(C). On the other hand, 3PF imaging modality not only exhibits less trachea-induced light distortion as shown in Fig. 2(D), but also benefits from better optical sectioning (Fig. 4), thus provides deeper imaging depth than 2PF. In contrast, the single-photon fluorescence images in Fig. 1(A) (see the white arrow) demonstrate loss of image contrast mainly due to scattering.

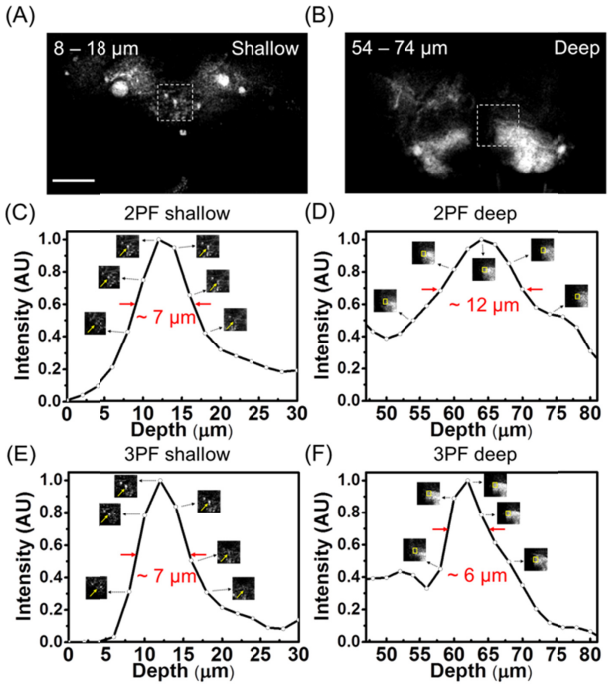

Fig. 4. Depth-dependent axial confinement of 2PF and 3PF inside a living *Drosophila* brain. (A) and (B) show the 3PF image stack projections at shallow (8 - 18 μm) and deep (54 - 74 μm) regions. The white-dashed boxes show the selected area for depth-dependent axial confinement analysis of (C) - (D) 2PF and of (E) - (F) 3PF. Comparing (C) and (E), which are at shallow region, the axial confinement of 2PF and 3PF are comparable, as manifested by the inset images at different depths. On the other hand, for (D) and (F) at deep region, the 3PF axial confinement is similar to that at shallow region, but the 2PF axial confinement is much worse. The underlying reason is the excess light distortion induced by trachea in a living brain, and the result is image blur for 2PF in deep brain region.

In Figs. 2(A) and 2(B), the trachea-contributed light distortion is more efficiently removed by degassing in the 2PF modality (~35% reduction) than 1PF (~24% reduction). In addition, from Fig. 2(D), μ_{tra} for 3PF are larger than μ_{neu}. These two observations further suggest that tracheae-contributed light distortion is the main factor to impede multiphoton deep-brain imaging in a living *Drosophila*.

As shown in Fig. 1 and Visualization 3, to reaching the milestone of *in vivo* whole-brain imaging in *Drosophila*, 3PF at 1300-nm should be the optimal choice. Here we quantify the depth limit of 3PF by analyzing its signal-to-background ratio (SBR) in Fig. 5(A) and 3(B), along with comparison between 2PF and 3PF. The SBR determination method was similar to a previous publication [22]. Briefly, the signal value was averaged from the pixels with top 1% intensities from the white box in inset of Fig. 2(A), and the background value was the average of all pixel intensities in the white box of Fig. 5(A), where no brain tissue was found

Biomedical Optics EXPRESS

throughout the whole depth range. With this definition, the signals mostly came from the in-focus regions, and the background arose from out-of-imaging-plane contributions. Both SBR results are normalized to the 2PF value at 100 μm depth, where no distinguishable features are observable.

In Fig. 5(B), the 2PF SBR reaches unity at ~100 μm, since no structure is distinguishable beyond this depth (Visualization 2), while the SBR of 3PF significantly outstands the former. The imaging depth of 3PF reaches at least 200 μm. The result once again supports that 3PF is capable to image through a whole *Drosophila* brain.

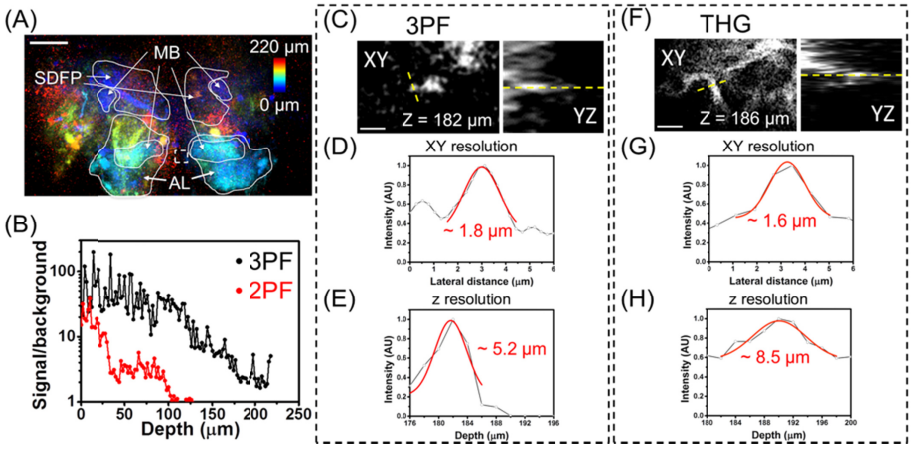

Fig. 5. Signal-to-background ratio (SBR) and resolution analysis. (A) Color-coded depth projection image of 3PF throughout the whole-brain, showing different structures at different depths. The white-dashed box in the center represents the region of background selection. (B) SBR of 2PF and 3PF signals at each depth at the same brain. (C) and (F) show the XY image of 3PF and THG at 182 and 186 μm, and their YZ images are given on the right-hand-side, respectively. The lateral resolutions are ~1.8 μm (D) for 3PF and ~1.2 μm (G) for THG signals. The axial resolutions are ~5.2 μm for 3PF (E) and ~6.5 μm for THG (H), respectively. Scale bars: 50 μm in (A), 5 μm in (C).

Having said the penetration depth limit of 2PF, please note that the dorsal-ventral length of a *Drosophila* brain is about 200 μm, but the anterior-posterior length is only slightly above 100 μm. In addition, the density of trachea develops with age [28]. Therefore, it is possible to perform whole-brain imaging through the anterior-posterior axis with a young adult *Drosophila*, as demonstrated recently [29], at the expense to remove olfactory sensory organs such as antennae and proboscis. In addition, from Fig. 1G in their work, at about 100 μm deep in the brain, only large neuropil structures such as calyx on the edge of the brain are visible, but the central area becomes unclear. Their results also manifest limited penetration capability of *in vivo* 2PF, and the number agrees well with our results.

The spatial resolutions of 3PF and THG in deep-brain region are given in Figs. 5(C) - 6(H). For 3PF, the minimal full-width-at-half-maximum (FWHM) is 1.8 μm laterally and 5.2 μm axially, which is sufficient to resolve a single cell in the *Drosophila* brain [30]. For THG, the FWHM is comparable, 1.6 μm in lateral and 8.5 μm in axial directions.

Another practical consideration is to avoid absorption-induce damage, since the pulse energy of 3P excitation is typically much higher than 2P excitation. It has been shown that 1300-nm excitation is less phototoxic than Ti: sapphire excitation at 800-nm [31]. In a recent work of 2PF [32], 120-mW average power at ~1300-nm does not induce any damage to a living mouse brain. In addition, a very recent work demonstrated 3PF functional imaging in mouse with ~1300-nm excitation [22]. Their average power is 50 mW, corresponding to 60-nJ pulse energy (800 kHz rep. rate), and demonstrated long-term viability of the experimental animals. In our 3PF imaging, maximally 20 mW average power is used at the bottom of brain, corresponding to ~50 nJ pulse energy (400 kHz rep. rate). Additionally, no noticeable damage

Biomedical Optics EXPRESS

was observed in the brain tissue experimentally. Since both the average power and pulse energy are lower than previous *in vivo* experiments, our imaging condition should allow living brain studies in *Drosophila*.

4. Conclusions

In conclusion, we have, for the first time, characterized the optical properties of the *Drosophila* brain, which is filled with air, with single-photon, two-photon, and three-photon modalities. We found that the main limiting factor that impedes *in vivo* whole-brain single-photon imaging is scattering, but for multiphoton imaging, light distortion from tracheae structures plays a more dominant role. The light distortion affects not only signal attenuation, but also image visibility. Although degassing enables whole-*Drosophila*-brain imaging by reducing trachea-induced light distortion, the only way to achieve *in vivo* whole-brain imaging with single cell resolution is 3PF at 1300-nm excitation, which exhibits less scattering, light distortion, and better optical sectioning. It is possible to combine with AO to further reduce light distortion [21], thus allowing deep-tissue imaging on the scale extending from a single neuron, a complete brain network, toward a whole-animal connectome [33].

Funding

Ministry of Science and Technology, Taiwan, (MOST-107-2321-B-002-009, MOST-105-2628-M-002-010-MY4 and MOST-104-2218-E-007-022-MY2); Brain Research Center under the Higher Education Sprout Project funded by the Ministry of Science and Technology and Ministry of Education in Taiwan.

Acknowledgments

The three-photon brain imaging cannot be done without the great help from Chris Xu and Tianyu Wang from School of Applied and Engineering Physics in Cornell University. In addition, we appreciate the generous support of transgenic *Drosophila* from Chun Han and Rushaniya Fazliyeva from Institute of Cell and Molecular Biology in Cornell University. SWC acknowledges the generous support from the Foundation for the Advancement of Outstanding Scholarship.

Disclosures

The authors declare that there are no conflicts of interest related to this article.

References

1. A.-S. Chiang, C.-Y. Lin, C.-C. Chuang, H.-M. Chang, C.-H. Hsieh, C.-W. Yeh, C.-T. Shih, J.-J. Wu, G.-T. Wang, Y.-C. Chen, C.-C. Wu, G.-Y. Chen, Y.-T. Ching, P.-C. Lee, C.-Y. Lin, H.-H. Lin, C.-C. Wu, H.-W. Hsu, Y.-A. Huang, J.-Y. Chen, H.-J. Chiang, C.-F. Lu, R.-F. Ni, C.-Y. Yeh, and J.-K. Hwang, "Three-dimensional reconstruction of brain-wide wiring networks in *Drosophila* at single-cell resolution," Curr. Biol. **21**(1), 1–11 (2011).
2. C.-T. Shih, O. Sporns, S.-L. Yuan, T.-S. Su, Y.-J. Lin, C.-C. Chuang, T.-Y. Wang, C.-C. Lo, R. J. Greenspan, and A. S. Chiang, "Connectomics-based analysis of information flow in the Drosophila brain," Curr. Biol. **25**(10), 1249–1258 (2015).
3. Z. Zheng, J. S. Lauritzen, E. Perlman, C. G. Robinson, M. Nichols, D. Milkie, O. Torrens, J. Price, C. B. Fisher, N. Sharifi, S. A. Calle-Schuler, L. Kmecova, I. J. Ali, B. Karsh, E. T. Trautman, J. A. Bogovic, P. Hanslovsky, G. S. X. E. Jefferis, M. Kazhdan, K. Khairy, S. Saalfeld, R. D. Fetter, and D. D. Bock, "A complete electron microscopy volume of the brain of adult *Drosophila* melanogaster," Cell **174**(3), 730–743 (2018).
4. F. Helmchen and W. Denk, "Deep tissue two-photon microscopy," Nat. Methods **2**(12), 932–940 (2005).
5. N. G. Horton, K. Wang, D. Kobat, C. G. Clark, F. W. Wise, C. B. Schaffer, and C. Xu, "*In vivo* three-photon microscopy of subcortical structures within an intact mouse brain," Nat. Photonics **7**(3), 205–209 (2013).
6. Y. Wang, H. F. Guo, T. A. Pologruto, F. Hannan, I. Hakker, K. Svoboda, and Y. Zhong, "Stereotyped odor-evoked activity in the mushroom body of *Drosophila* revealed by green fluorescent protein-based Ca^{2+} imaging," J. Neurosci. **24**(29), 6507–6514 (2004).
7. K. S. Honegger, R. A. A. Campbell, and G. C. Turner, "Cellular-resolution population imaging reveals robust sparse coding in the *Drosophila* mushroom body," J. Neurosci. **31**(33), 11772–11785 (2011).

Biomedical Optics EXPRESS

8. J. W. Wang, A. M. Wong, J. Flores, L. B. Vosshall, and R. Axel, "Two-photon calcium imaging reveals an odor-evoked map of activity in the fly brain," Cell **112**(2), 271–282 (2003).
9. C. M. Root, J. L. Semmelhack, A. M. Wong, J. Flores, and J. W. Wang, "Propagation of olfactory information in *Drosophila*," Proc. Natl. Acad. Sci. U.S.A. **104**(28), 11826–11831 (2007).
10. R. Ignell, C. M. Root, R. T. Birse, J. W. Wang, D. R. Nässel, and Å. M. E. Winther, "Presynaptic peptidergic modulation of olfactory receptor neurons in *Drosophila*," Proc. Natl. Acad. Sci. U.S.A. **106**(31), 13070–13075 (2009).
11. V. Ruta, S. R. Datta, M. L. Vasconcelos, J. Freeland, L. L. Looger, and R. Axel, "A dimorphic pheromone circuit in *Drosophila* from sensory input to descending output," Nature **468**(7324), 686–690 (2010).
12. G. J. Beitel and M. A. Krasnow, "Genetic control of epithelial tube size in the *Drosophila* tracheal system," Development **127**(15), 3271–3282 (2000).
13. L. Wei, Z. Chen, and W. Min, "Stimulated emission reduced fluorescence microscopy: a concept for extending the fundamental depth limit of two-photon fluorescence imaging," Biomed. Opt. Express **3**(6), 1465–1475 (2012).
14. P. Theer, M. T. Hasan, and W. Denk, "Two-photon imaging to a depth of 1000 microm in living brains by use of a Ti:Al2O3 regenerative amplifier," Opt. Lett. **28**(12), 1022–1024 (2003).
15. J. Tang, R. N. Germain, and M. Cui, "Superpenetration optical microscopy by iterative multiphoton adaptive compensation technique," Proc. Natl. Acad. Sci. U.S.A. **109**(22), 8434–8439 (2012).
16. M. J. Booth, "Adaptive optical microscopy: the ongoing quest for a perfect image," Light Sci. Appl. **3**(4), e165 (2014).
17. C. Wang, R. Liu, D. E. Milkie, W. Sun, Z. Tan, A. Kerlin, T.-W. Chen, D. S. Kim, and N. Ji, "Multiplexed aberration measurement for deep tissue imaging *in vivo*," Nat. Methods **11**(10), 1037–1040 (2014).
18. M. Pedrazzani, V. Loriette, P. Tchenio, S. Benrezzak, D. Nutarelli, and A. Fragola, "Sensorless adaptive optics implementation in widefield optical sectioning microscopy inside *in vivo Drosophila* brain," J. Biomed. Opt. **21**(3), 036006 (2016).
19. S.-W. Chu, S.-Y. Chen, T.-H. Tsai, T.-M. Liu, C.-Y. Lin, H.-J. Tsai, and C.-K. Sun, "*In vivo* developmental biology study using noninvasive multi-harmonic generation microscopy," Opt. Express **11**(23), 3093–3099 (2003).
20. D. Kobat, N. G. Horton, and C. Xu, "*In vivo* two-photon microscopy to 1.6-mm depth in mouse cortex," J. Biomed. Opt. **16**(10), 106014 (2011).
21. X. Tao, H.-H. Lin, T. Lam, R. Rodriguez, J. W. Wang, and J. Kubby, "Transcutical imaging with cellular and subcellular resolution," Biomed. Opt. Express **8**(3), 1277–1289 (2017).
22. D. G. Ouzounov, T. Wang, M. Wang, D. D. Feng, N. G. Horton, J. C. Cruz-Hernández, Y.-T. Cheng, J. Reimer, A. S. Tolias, N. Nishimura, and C. Xu, "*In vivo* three-photon imaging of activity of GCaMP6-labeled neurons deep in intact mouse brain," Nat. Methods **14**(4), 388–390 (2017).
23. H.-H. Lin, L.-A. Chu, T.-F. Fu, B. J. Dickson, and A.-S. Chiang, "Parallel neural pathways mediate CO_2 avoidance responses in *Drosophila*," Science **340**(6138), 1338–1341 (2013).
24. C.-W. Lin, H.-W. Lin, M.-T. Chiu, Y.-H. Shih, T.-Y. Wang, H.-M. Chang, and A.-S. Chiang, "Automated *in situ* brain imaging for mapping the *Drosophila* connectome," J. Neurogenet. **29**(4), 157–168 (2015).
25. N. Ji, T. R. Sato, and E. Betzig, "Characterization and adaptive optical correction of aberrations during in vivo imaging in the mouse cortex," Proc. Natl. Acad. Sci. U.S.A. **109**(1), 22–27 (2012).
26. E. Chaigneau, A. J. Wright, S. P. Poland, J. M. Girkin, and R. A. Silver, "Impact of wavefront distortion and scattering on 2-photon microscopy in mammalian brain tissue," Opt. Express **19**(23), 22755–22774 (2011).
27. C.-Y. Dong, K. Koenig, and P. So, "Characterizing point spread functions of two-photon fluorescence microscopy in turbid medium," J. Biomed. Opt. **8**(3), 450–459 (2003).
28. P. R. Rao, L. Lin, H. Huang, A. Guha, S. Roy, and T. B. Kornberg, "Developmental compartments in the larval trachea of *Drosophila*," eLife **4**, e08666 (2015).
29. K. Mann, C. L. Gallen, and T. R. Clandinin, "Whole-brain calcium imaging reveals an intrinsic functional network in *Drosophila*," Curr. Biol. **27**(15), 2389–2396 (2017).
30. J. C. Tuthill, "Lessons from a compartmental model of a *Drosophila* neuron," J. Neurosci. **29**(39), 12033–12034 (2009).
31. I. H. Chen, S. W. Chu, C. K. Sun, P. C. Cheng, and B. L. Lin, "Wavelength dependent damage in biological multi-photon confocal microscopy: A micro-spectroscopic comparison between femtosecond Ti:sapphire and Cr:forsterite laser sources," Opt. Quantum Electron. **34**(12), 1251–1266 (2002).
32. D. Kobat, M. E. Durst, N. Nishimura, A. W. Wong, C. B. Schaffer, and C. Xu, "Deep tissue multiphoton microscopy using longer wavelength excitation," Opt. Express **17**(16), 13354–13364 (2009).
33. C.-C. Lo and A.-S. Chiang, "Toward whole-body connectomics," J. Neurosci. **36**(45), 11375–11383 (2016).